

# Retrofitting of Reinforced Concrete Beam-Column via Steel Jackets against Close-in Detonation

Swee Hong TAN, Jiing Koon POON, Roger CHAN and David CHNG

*Ministry of Home Affairs, Singapore*

## Abstract

*This paper presents results from simulation, in comparison to findings from full-scale blast trials of Reinforced Concrete Beam-Column test specimens. 2 numerical approaches were adopted. First method was a 2-stage approach which involved applying segment pressure loadings, derived from Computational Fluid Dynamics (CFD) calculations, on LS-DYNA<sup>®</sup> Lagrangian models to predict structural response. Second method was the use of \*Load\_Blast\_Enhanced keyword to couple empirical blast loads to air domain in Arbitrary Lagrangian-Euler (ALE) environment for direct LS-DYNA Fluid-Structure Interaction (FSI) computations. Grid Convergence Index (GCI) principles were used to check adequacy of mesh refinement studies.*

## 1. Introduction

In an urban environment, buildings enjoy little stand-off distance from external roads and often have basement parking facilities. Such setting may be exploited by adversaries who would want to create mass casualties by causing collapse of the building. For structures that lack redundancy to resist the initial loss of a key element, progressive collapse may occur. Progressive collapse is defined as the spread of an initial local failure from element to element, resulting eventually in the collapse of an entire structure or disproportionately large part of it [1]. From a civilian protective security point of view, understanding structural response against close in, contact and/or near contact detonation effects is therefore of utmost importance.

Use of steel jacketing to retrofit reinforced concrete columns is an established industry practice to enhance structural resilience of bridge columns against extreme seismic requirements [2]. The concept works by allowing concrete to develop confined strength which improves the overall load carrying capacity of the structural element.

Similar approach is also widely adopted in the context of civilian protective security. Typical analytical methodologies which security practitioners use for retrofit designs are based on Single-Degree-Of-Freedom (SDOF) and/or Multi-Degree-Of-Freedom (MDOF) idealizations [3]. It is emphasized that simplified approximations have their limitations due to assumed structural response modes, component interactions and blast loads [4]. In a nutshell, contact and/or near contact scenarios are situations which are not expected to be adequately covered by SDOF and/or MDOF. There are no definitive design methodologies with respect to steel jacket retrofitting against near-field blast effects from open source codes, standards and guidelines.

This paper presents results from simulation in comparison to a recently concluded test series by Singapore Ministry of Home Affairs (MHA). This series was the second part of a long-term technology development programme embarked by MHA, to study close in, contact and/or near contact blast effects on structural elements as well as the mechanism of progressive collapse. The first part was reported in 82<sup>nd</sup> SAVIAC (2011) by David Chng et al. [5] and Liang S.W. et al. [6]. The focus of this paper is to discuss about the simulation techniques considered for such areas of interests, including preliminary observations pertaining to the use of \*LOAD\_BLAST\_ENHANCED (LBE) with Multi-Material Arbitrary Lagrange Eulerian (MM-ALE) solver. MHA also looks into other critical aspects of protective security, which include hostile vehicle mitigation using anti-ram barriers. Tay S.K. et al. [7] had adopted similar LS-DYNA Lagrangian techniques. Simulation results had compared well with actual impact tests on security bollards.

The procedures discussed in this paper are not meant to be a full illustration of verification and validation procedures [8,9]. The ASME Guide for Computational Solid Mechanics highlighted the importance of a “Bottom-Up” approach. A hierarchical structure of physical systems needs to be mapped out before starting verification and validation workflow from lower tier towards final level of intended use. This would involve material characterization tests at component level. While solution verification via estimation of numerical errors associated with discretization is critical, sources of errors in validation experiments must not be neglected.

## 2. Full-Scale Blast Trials

This series of full-scale blast trials was carried out in an arena format in which four beam-column specimens were placed around the charge weight in a single detonation. As these specimens were located in close proximity to one another, prior analyses via CFD calculations were carried out to ensure that the intended arrangement would not have significant influence on the blast propagation (as opposed to a hypothetical scenario whereby only a single specimen is tested). The charge was a spherical shape of cast Trinitrotoluene (TNT) explosives, elevated from ground level using Styrofoam panels. Instrumentation employed were high-speed cameras and free-field incident pressure gauges strategically placed at the test site, as well as one pressure gauge per beam-column specimen, placed at mid-span to record reflected pressure-time history profile. To minimize the likelihood of hard stones hitting these pressure gauges mounted on specimens, the top soil of the test site was replaced with sand. Before detonation, every beam-column specimen was pre-loaded with 50 tons axial force by a system of hydraulic jacks and steel rods. After blast, these specimens were subjected to compression on site by a customized compression rig to establish the post-blast residual strength of each beam-column.

Figure 1 compares the un-retrofitted beam-columns against retrofitted ones. The steel jacketing retrofit design had limited the overall structural lateral response and had prevented the disengagement of the concrete due to localized effects, such as breach and spall.



BEFORE Retrofitting (Front View)



BEFORE Retrofitting (Back View)



AFTER Retrofitting: Scenario 1



AFTER Retrofitting: Scenario 2

**Figure 1: Post-blast photographs (Un-retrofitted versus Retrofitted)**

Two scenarios were chosen as case studies for this paper, termed as Scenario 1 and Scenario 2. The only difference between the two was that the stand-off distance for the specimen in Scenario 1 was further than that for specimen in Scenario 2. The specimens used in both scenarios were 300 mm x 300 mm reinforced concrete element retrofitted with 6 mm thick steel jackets bolted together along the length of element and anchored with base-plates at both ends.

### 3. Overview of Lagrange Model in LS-DYNA

Figure 2 shows the Lagrange model in LS-DYNA, created to be symmetrical about the mid-span of beam-column. The pre & post-processor used was LS-PrePost®. Displacement and rotational restraints were imposed on all mid-span nodes to represent the region of counter-flexure. 10 mm, 20 mm and 50 mm mesh configurations were studied. Due to geometrical complexity of the problem, only the concrete, steel reinforcement and anchor bolts elements were modeled exactly to the intended mesh sizes, while that of steel jacket and tied bolts were meshed as close as possible to the intended sizes.

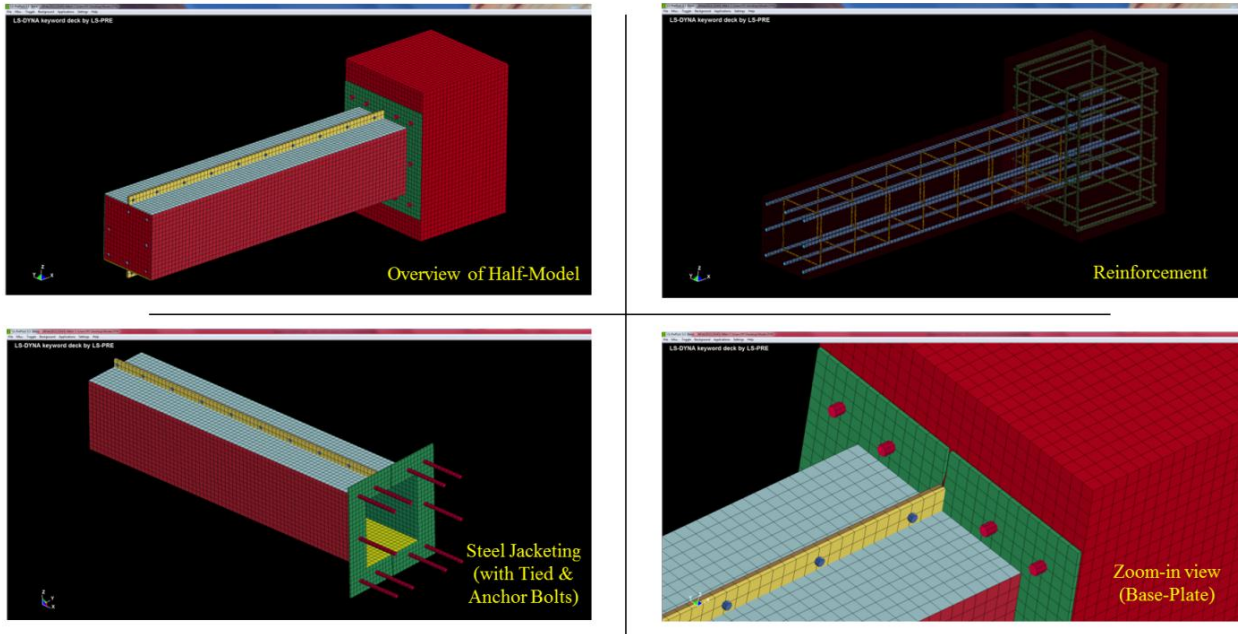


Figure 2: Lagrange model in LS-DYNA created using LS-PrePost

Concrete was represented by 8-nodes constant stress solid elements. Two material models were employed, \*MAT\_72R3 (\*MAT\_CONCRETE\_DAMAGE\_REL3) and \*MAT\_159 (\*MAT\_CSCM\_CONCRETE). Auto-generation of parameters was based on unconfined compressive cylinder strength of 33.34 MPa (which correlates approximately with 40 MPa cube strength [10]). Maximum aggregate size of 20 mm was normalized across these models, via LOCWID in \*MAT\_72R3 and DAGG in \*MAT\_159 respectively. Mass density was kept the same. Two hourglass control types were used interchangeably. Viscous based hourglass control Type 3 was used for blast, while stiffness based hourglass control Type 5 was used for pre-load and post-blast compression. It is vital that the correct hourglass control is used. A stiffness based method would produce unrealistic damage accumulation when used in high loading rate problem, such as impulsive blast.

Steel reinforcement was represented by beam elements (Hughes-Liu with cross section integration). \*MAT\_24 (\*MAT\_PIECEWISE\_LINEAR\_PLASTICITY) was used in tandem with a series of true stress-strain curves estimated from the base engineering stress-strain curve and the Dynamic Increase Factor (DIF) for both yield and ultimate conditions reported by Malvar L. J. [11]. ASTM A615 Grade 60 steel with nominal yield strength at 414 MPa was assumed for the 460 MPa reinforcement used in the test. \*CONSTRAINED\_LAGRANGE\_IN\_SOLID keyword with CTYPE = 2 was used to couple concrete and reinforcement actions. In absence of material characterization data for tied and anchors bolts, the same was assumed for Grade 8.8 non-preloaded bolts with shear strength of 375 MPa and tension strength of 560 MPa [12].

The failure criterion allowable in \*MAT\_24 is only that of plastic strain. Besides axial deformation, shear failure mode was deemed equally important and had to be adequately accounted for. For current studies, the tied and anchors bolts faced higher shear demands than steel reinforcement within the concrete. At the moment, axial and shear checks were done manually. Plastic strain outputs were compared against average ultimate strain. Resultant forces

at the interfaces between tied and anchor bolts to the steel jackets were plotted and checked against allowable shear capacity of bolts (established by shear strength of 375 MPa with assumed DIF). Notwithstanding the fact that the material properties were not exact in the first place, these pre-trial axial strain and shear checks were necessary to predict if the steel jackets would open up at the tied bolt interfaces or dislodged from the end block due to failure of anchor bolts.

Steel jacket was represented by fully integrated shell elements with IHQ = 8 activated for full projection warping stiffness in hourglass control. ASTM A572 Grade 50 steel with nominal yield strength at 345 MPa was assumed for 355 MPa structural steel used in the test. Similar concept of deriving a series of true stress-strain curves from DIF for both yield and ultimate conditions reported by Malvar L. J. was used with \*MAT\_24, except that the base engineering stress-strain curve was extracted from ASM International publication [13]. The DIF reported by Malvar L. J. were derived based on experimental data from laboratory tests done on reinforcing bars, and not structural steel plates. Two possible alternatives are first, the use of DIF for structural steel from UFC 3-340-02 [14] to develop a series of true stress-strain curves, and second, the use of Cowper-Symonds hardening model using parameters recommended in Research Report 435 by UK Steel Construction Institute [15]. Steel jacket, tied and anchor bolts shared nodes at the required specific interfaces. \*CONSTRAINED\_LAGRANGE\_IN\_SOLID keyword with CTYPE = 2 was used to represent anchor bolts embedded with concrete end blocks.

Two categories of contact keywords were used. First was \*CONTACT\_AUTOMATIC\_SURFACE\_TO\_SURFACE to account for the interaction at the top and bottom “fins” of the steel jacket as well as that between the base-plates with the concrete end blocks. Second was \*CONTACT\_AUTOMATIC\_SURFACE\_TO\_SURFACE\_TIEBREAK with OPTION = 5 to represent the epoxy bonding between steel jacket and the concrete. A series of arbitrary small-scale problems were created to verify if delamination could occur at the correct interface forces, and this provided confidence that epoxy’s adhesive properties were sufficiently captured.

#### 4. Stage 1 – Derivation of Blast Loads

CFD calculations were performed in ANSYS<sup>®</sup> AUTODYN to derive the pressure-time history at various specific locations along the beam-column.

Figure 3 shows a screen-shot of the CFD model, including eight gauges placed to capture the pressure-time history at specific locations along the beam-column. The beam-column was created by “unused space” in order to represent a non-responding structure in the blast propagation environment. Close-in detonation is in the impulsive loading regime of structure whereby significant structure response would only set in after the blast wave has passed.

Figure 4 shows impulse results captured at mid-span gauge for both Scenario 1 and 2 using different mesh configurations ( $I_{100}$  represents impulse for 100 mm mesh size, and so on). Solution verification in terms of Grid Convergence Index (GCI) calculations is also presented. Extrapolated value based on the Richardson Extrapolation (RE) principles agree well with field measurement obtained. GCI of 4.69% and 9.74% for Scenario 1 and 2 respectively may mean that convergence has been reasonably achieved. All runs under Scenario 1 were within 5%

energy error (a term used in ANSYS AUTODYN to quantify energy loss due to numerical procedures), while runs under Scenario 2 range from between 5% to 10%.

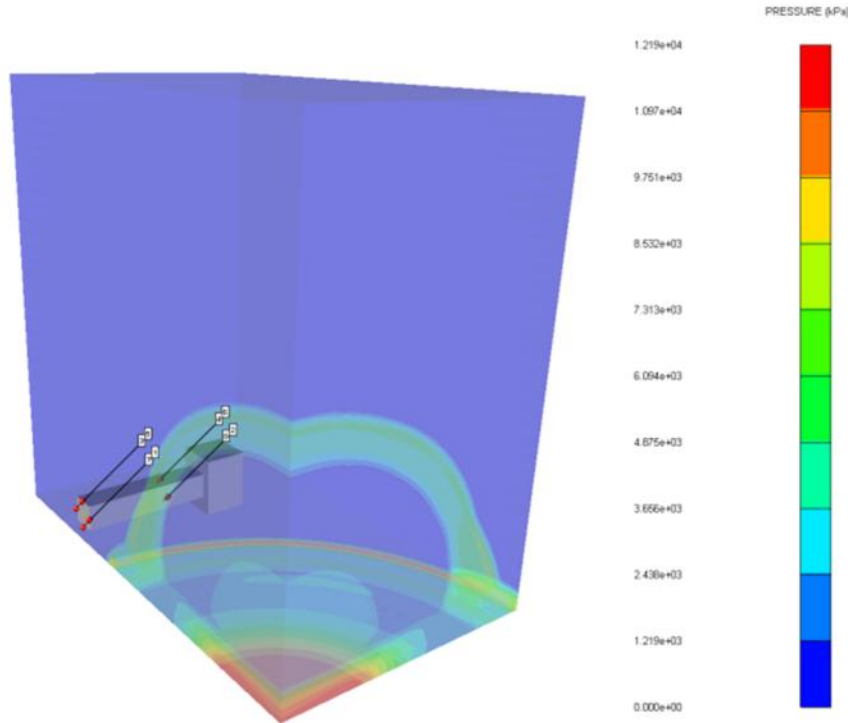


Figure 3: ANSYS AUTODYN model for CFD calculations

	Impulse at Mid-Span (kPa)				$p$	GCI <sub>50/75</sub>	95% Confidence Interval
	$I_{100}$	$I_{75}$	$I_{50}$	$I_{\text{Extrapolated}}$			
Scenario 1	10607	10756	11312	11736	2.066	0.04687	[ 10781 , 11842 ]
			Measured	12914			

	Impulse at Mid-Span (kPa)				$p$	GCI <sub>30/50</sub>	95% Confidence Interval
	$I_{75}$	$I_{50}$	$I_{30}$	$I_{\text{Extrapolated}}$			
Scenario 2	14023	14808	15476	16681	0.8629	0.0974	[ 13968 , 16983 ]
			Measured	16292			

Figure 4: Mesh refinement studies for Impulse at mid-span

### 5. Stage 2 - Lagrangian Simulation

This stage consisted of 3 phases, i.e. 50 tons pre-load, blast and post-blast compression to failure, achieved by invoking full restart function using \*STRESS\_INITIALIZATION keyword.

Pre-load phase involved applying prescribed boundary displacement to nodes of extreme surface of concrete end block in the direction towards the mid-span. Initial estimate of the displacement

required to reach 50 tons was computed using equations reported by James G. MacGregor et al. [16]. As the response was expected to be within elastic limit, based on results from the first run using initial estimate, a second run using proportionally adjusted displacement value was conducted to yield an exact 50 tons cross-sectional force within beam-column. The time over which the displacement value was applied, was more than two times of the estimated natural period of the axial response of the beam-column so as to simulate a near quasi-static rate of loading.

Blast phase involved applying sets of triangular load (idealized based on impulse from AUTODYN results) as segment loadings on beam-column. Such load simplification is permitted by ASCE Standard 59-11 for close-in effect calculations, whereby the pulse duration is short relative to the natural period of the structural element. Natural period of flexural response was obtained from free vibration mode simulation before adding \*DAMPING\_GLOBAL keyword to signify 1% of critical damping (via parameter VALDMP) to input file.

Post-blast compression phase was similar to the pre-load phase. Prescribed boundary displacement to nodes of extreme surface of concrete end block was further increased until sum of axial forces at the mid-span nodes, i.e. contribution from concrete, steel jacket and reinforcement, reached a maximum. There was a reference beam-column subjected to only axial compression till failure (right from start without undergoing blast). Numerical simulation was also carried out for this single pure compression test. Experimental finding tallied well with empirical calculation based on equations reported by James G. MacGregor et al. It also fell reasonably within range of measured capacities from simulation, i.e. concrete only contribution (lower bound) and summation of contribution from both concrete and reinforcement (upper bound). It was worth noting that \*MAT\_72R3 and \*MAT\_159 yielded almost identical results, as seen from Figure 5.

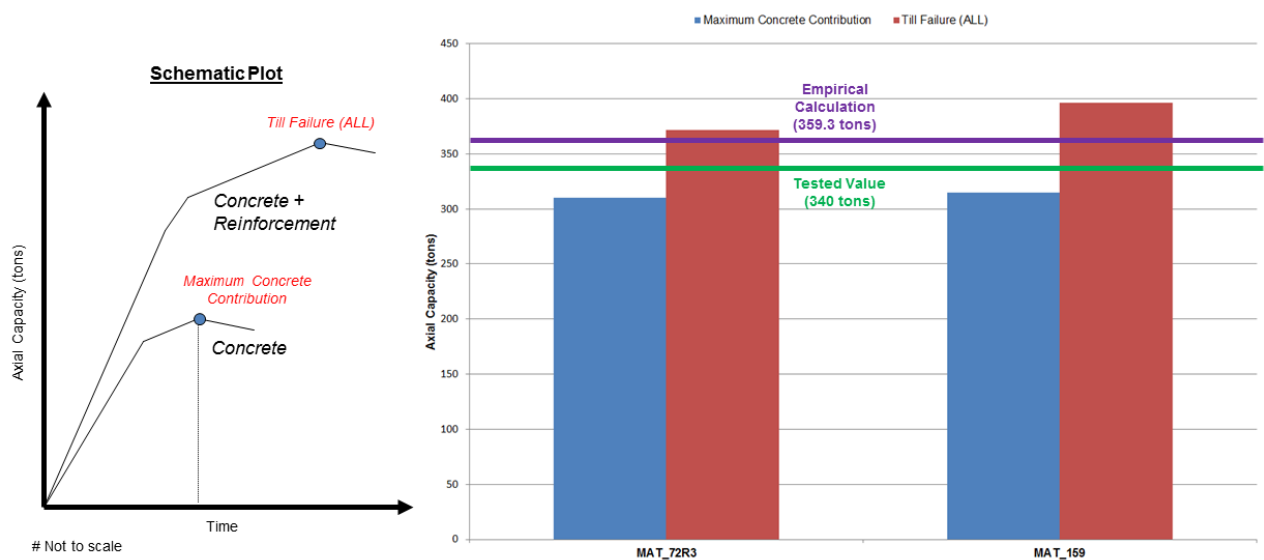


**Figure 5:** Axial capacity simulation results for compression test on reference specimen (20mm mesh)

## 6. Results from Lagrangian Simulation

Figure 6 shows the mid-span displacement profiles calculated for Scenario 1 and 2 for both concrete material models. The hourglass energy for \*MAT\_72R3 was consistently higher than that in \*MAT\_159 and hovered around 10% of the internal energy, which could be considered acceptable for such complex problems. Both peak displacement and permanent mid-span plastic deformation computed using \*MAT\_72R3 were higher than that in \*MAT\_159. The field measurements obtained were counter-intuitive. Scenario 1, at a further stand-off distance than Scenario 2, had resulted in a higher permanent plastic deformation. Putting this observation aside, simulation results were in same order of magnitude as field measurements.

Figure 7 compares the post-blast residual axial capacities calculated for Scenario 1 and 2 for both concrete material models. The extrapolated value for \*MAT\_159 for both scenarios agreed well with the measurements. Unlike simulation for reference specimen whereby both concrete material models fared almost equally, \*MAT\_159 clearly performed stronger than \*MAT\_72R3.

The inherent difference in tri-axial behavior at high confining pressure could be one of many possible reasons to explain the above-mentioned observations. \*MAT\_159 had converged better than \*MAT\_72R3 during both phases consistently. It was reasonable, on account these post-blast compression solutions depended on outcome of earlier blast simulations. Nevertheless, it has again been proven that same unconfined compressive strength in different concrete material models with automatic parameter generation capability may produce dissimilar results. In absence of detailed material characterization data, different concrete material models can be used to obtain a range of results. The need for characterization was also mentioned by J. M. Magallanes et al. [17] and it was further stated that the shear strength of concrete can be quite variable especially for confining pressures greater than 50 MPa.

Figure 6 & Figure 7 also tabulate the GCI calculations done for blast & post-blast phases respectively. Judging from the values obtained, it appears that potential limitations associated with existing discretization error estimate techniques due to severe nonlinearities as mentioned in ASME Guide for Computational Solid Mechanics exist. Notwithstanding possible “lack of rigorous theory for guidance in these situations” as reported in ASME Guide for Computational Solid Mechanics to adequately quantify mesh convergence, simulations using varying mesh sizes should still be carried out so as to appreciate extent of mesh sensitivity for the particular problem.

## 7. \*LOAD\_BLAST\_ENHANCED on MM-ALE Method

Use of “LBE on MM-ALE” method had been reported in several past papers, such as by Slavik, T. [18] and Len Schwer [19]. Preliminary observations when applying the “LBE on MM-ALE” method for current studies are:

- It appeared that there is no suitable boundary condition to account for outflow of shock waves. The present \*BOUNDARY\_NON\_REFLECTING appeared to be only valid for acoustics waves. One possible solution is to have the boundaries as far as possible from the beam-column model. Also, in order to prevent “contamination” from the expansion

waves due to atmospheric pressure condition at the boundaries (as set by PREF in \*CONTROL\_ALE), a full beam-column model (instead of half-model in earlier Lagrangian simulation) in a sizable air domain may be more appropriate.

- It seemed that there is no proper way to quantify fluid leakage due to interaction between beam-column and air, i.e. by comparing leakage control forces against main penalty coupling forces. Unlike a simple case whereby shell elements can be separately coupled with respective ALE Multi-Material Group (AMMG) on either side, doing the same for solid elements, i.e. couple concrete only against air outside its initial geometry, does not appear to be correct as the beam-column does not deform in tandem with movement of AMMGs. Visual appreciation of fluid leakage is still possible.
- It is difficult to account for advection loss in LBE as opposed to pure MM-ALE cases whereby the energy ratio can be tracked easily. For LBE, once blast reaches the receptor layer of air, energy ratio shoots up and goes into oscillation and it is unclear how to interpret this observation. An indirect way of checking is to place tracers in specific locations of air domain and compare against known results from established charts, such as UFC 3-340-02, wherever possible.
- The Mach Stem feature does not seem to be valid for close-in detonation cases, especially if the spherical charge is located close to ground level, as evident from the warning messages. Hence, for such situation, either one ignores the elevated placement of charge and assumes a hemispherical burst, or else one has to adopt a pure MM-ALE approach instead of the LBE method.

Most of above-mentioned observations are also relevant to pure MM-ALE runs. Detailed simulation results and associated parametric studies would be presented in next year's conference, if possible.

## 8. Conclusions

This paper presents results from simulation in comparison to a recently concluded test series by Singapore MHA. This series was the second part of a long-term technology development programme embarked by MHA, to study close in, contact and/or near contact blast effects on structural elements as well as the mechanism of progressive collapse.

Useful insights were gained from pre-test numerical simulations conducted and these would form part of the considerations for future work. Further in-depth studies are required in verification and validation aspects.

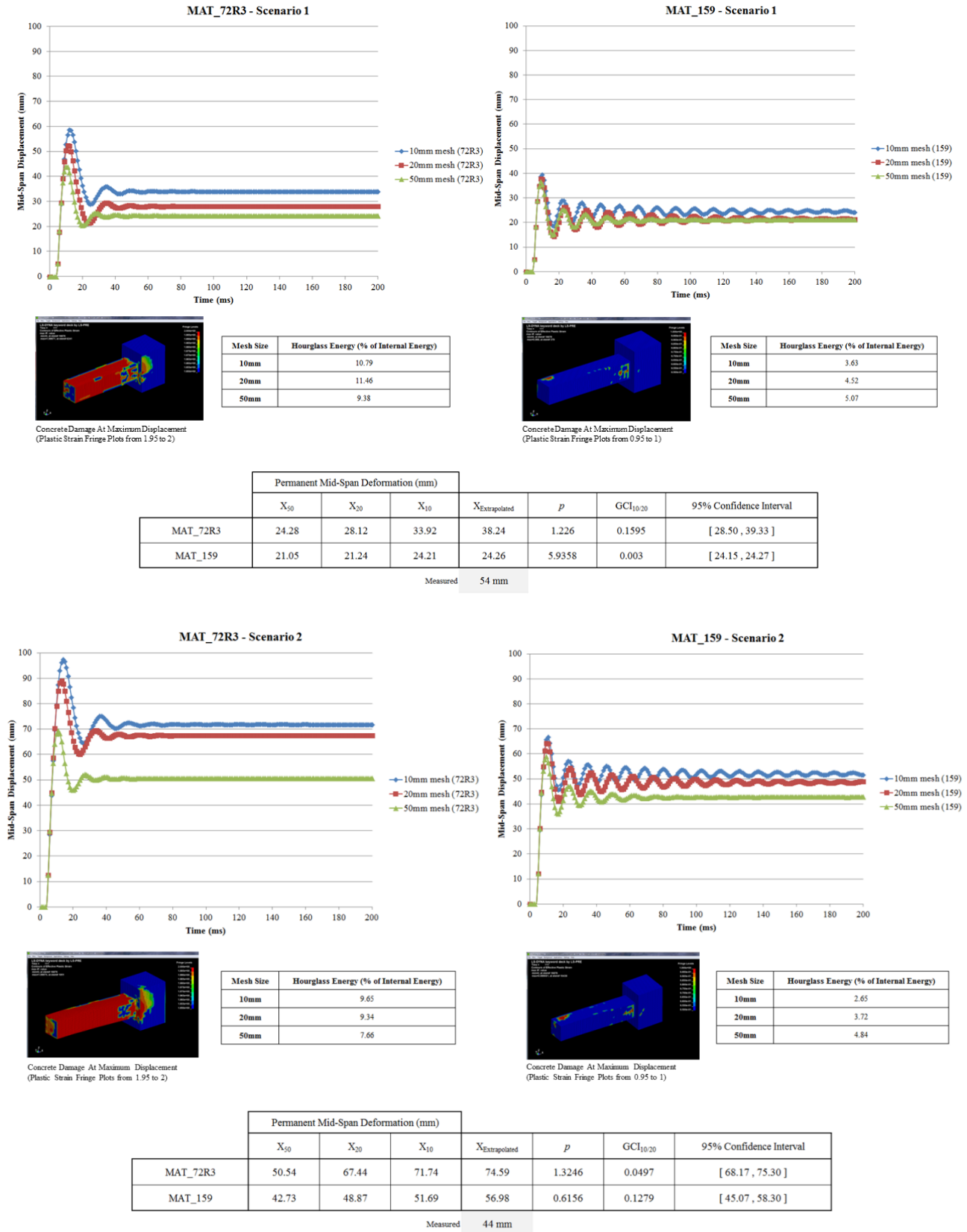


Figure 6: Mid-span displacement simulation results for Scenario 1 & 2

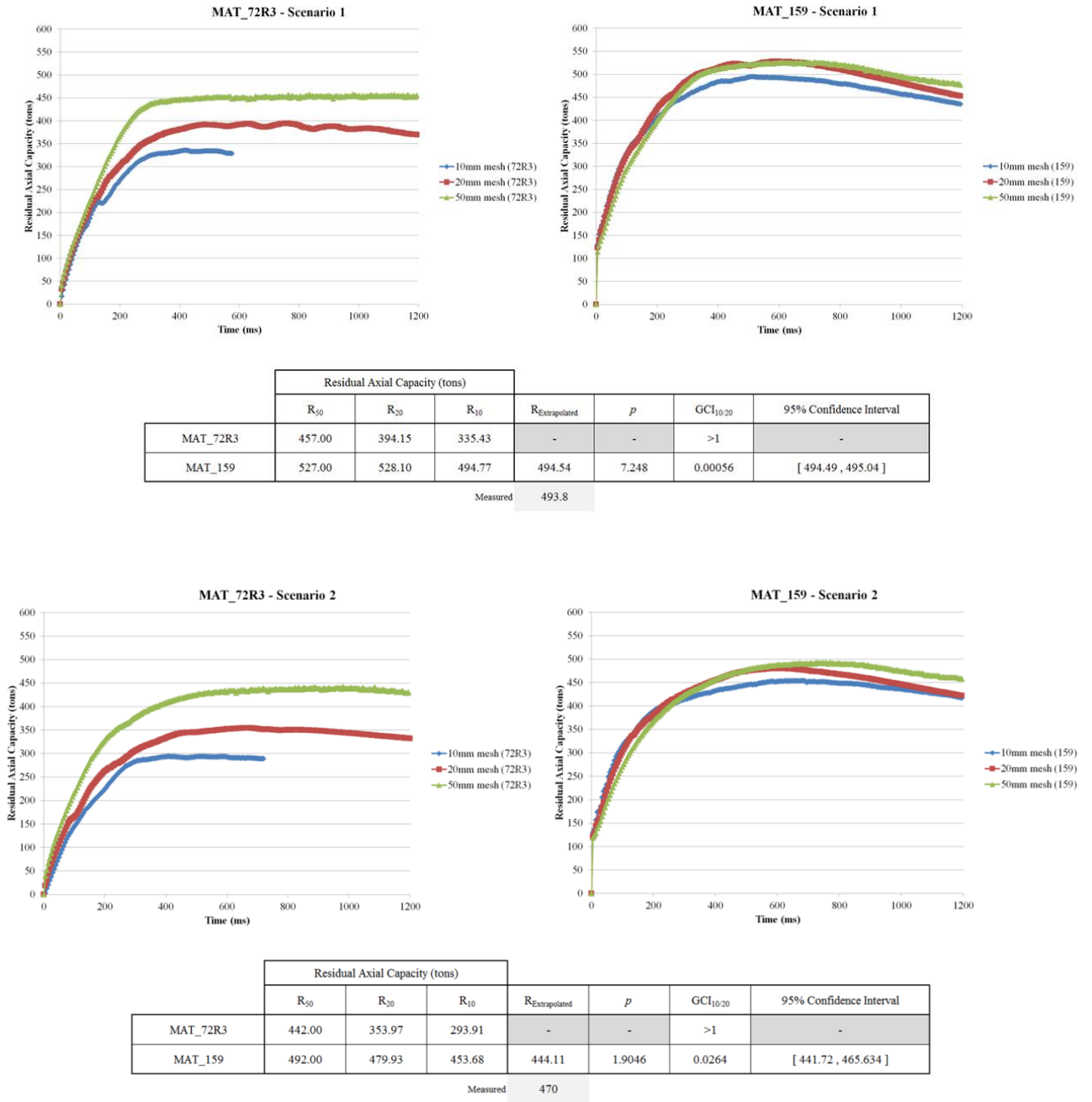


Figure 7: Post-blast residual axial capacity simulation results for Scenario 1 & 2

## 9. References

- [1] ASCE Standard 7-10. Minimum Design Loads for Buildings and Other Structures, 2010
- [2] Priestley, M. J. N., F. Seible and G. M. Calvi, Seismic Design and Retrofit of Bridges, John Wiley and Sons, NY, 1996
- [3] ASCE Standard 59-11. Blast Protection of Buildings, 2011
- [4] USACE PDC-TR 06-02. User's Guide for the Single-Degree-of-Freedom Blast Effects Design Spreadsheets (SBEDS), 2006
- [5] David Chng, Liang S.W., Bryan Lim, "Investigation of Residual Axial Capacities of Reinforced Concrete Beam-Columns Subjected to Blast Loads", 82<sup>nd</sup> Shock & Vibration Symposium, 2011
- [6] Liang S.W., Bryan Lim, Ng S.H., "Validation of Reinforced Concrete Column Subjected to Simultaneous Axial and Blast Loading", 82<sup>nd</sup> Shock & Vibration Symposium, 2011
- [7] Tay S.K., Bryan Lim, Ng S.H., "Crash Impact Modeling of Security Bollard", 12<sup>th</sup> International LS-DYNA Users Conference, 2012
- [8] ASME V&V 10-2006. Guide for Verification and Validation in Computational Solid Mechanics
- [9] ASME V&V 20-2009. Standard for Verification and Validation in Computational Fluid Dynamics and Heat Transfer
- [10] BS EN 1992-1-1:2004. Eurocode 2: Design of Concrete Structures – Part 1-1: General rules and rules for buildings
- [11] Malvar, L. J., "Review of Static and Dynamic Properties of Steel Reinforcing Bars," ACI Materials Journal, Volume 95, No. 5, September-October 1998, Page 609 - 616
- [12] BS 5950-1:2000. Structural use of steelwork in building – Part 1: Code of practice for design – Rolled and welded sections
- [13] ASM International, The Materials Information Society. Atlas of Stress-Strain Curves, 2<sup>nd</sup> Edition, 2002
- [14] UFC 3-340-02 (5 December 2008). Unified Facilities Criteria (UFC): Structures to Resist the Effects of Accidental Explosions
- [15] UK Steel Construction Institute for the Health and Safety Executive 2006. Improved Simplified Response Methods to Blast Loading, Research Report 435
- [16] James G. MacGregor, James K. Wright. Reinforced Concrete Mechanics and Design, Fourth Edition in SI Units, 2006
- [17] J. M. Magallanes, Y. C. Wu, L. J. Malvar, J. E. Crawford, "Recent Improvements to Release III of the K&C Concrete Model", 11<sup>th</sup> International LS-DYNA Users Conference, 2010
- [18] Slavik, T. "A Coupling of Empirical Explosive Blast Loads to ALE Air Domains in LS-DYNA", 7<sup>th</sup> European LS-DYNA Conference, 2009
- [19] Len Schwer. "A Brief Introduction to Coupling Load Blast Enhanced with Multi-Material ALE: The Best of Both Worlds for Air Blast Simulation", German LS-DYNA Forum, 2010